Astron. Astrophys. 351, 233–246 (1999)

ASTRONOMY AND ASTROPHYSICS

Molecular evolution in protoplanetary disks

Two-dimensional distributions and column densities of gaseous molecules

Y. Aikawa[1] **and E. Herbst**[2]

[1] Department of Physics, The Ohio State University, Columbus, OH 43210, USA (aikawa@pacific.mps.ohio-state.edu)
[2] Departments of Physics and Astronomy, The Ohio State University, Columbus, OH 43210, USA (herbst@mps.ohio-state.edu)

Received 19 July 1999 / Accepted 27 August 1999

Abstract. We investigate the two-dimensional (R, Z) distribution of molecules in circumstellar disks around young stellar objects. In the Z-direction, the disk can be schematically divided into three layers: the midplane, the outermost surface region, and the intermediate region. On the midplane, in cool outer regions of a disk, most of the molecules are adsorbed onto grains within a short time and depleted from the gas phase owing to the high density. As the height Z increases, the density decreases and the time scale for adsorption of molecules onto the dust particles increases. At the outermost surface regions, on the other hand, molecules are dissociated by UV radiation. Hence, in disks with a typical age (10^5–10^6 yr), molecular abundances have their peak values at some intermediate region. The height at which the abundances reach their peak values varies with species. Radicals, such as CN and C_2H, have their peaks at larger heights Z than more stable species such as HCN and NH_3. At significant distances from the midplane, the chemistry is also affected by a higher ionization rate due to X-rays, if the central star is a strong X-ray emitter, while, in the midplane, cosmic-rays are the main sources of ionization. The abundances of some species (e.g. HCN) are enhanced by a higher ionization rate.

Integrating molecular abundances perpendicular to the midplane, we obtain column densities for molecules, and their radial distribution. Column densities of selected molecules such as HNC and NH_3 are particularly sensitive to the total column density of the disk and the variation in UV radiation field due to the growth and sedimentation of dust particles. Our results show reasonable agreement with molecular abundances in the DM Tau disk estimated from radio observations.

Key words: solar system: formation – stars: circumstellar matter – stars: pre-main sequence – ISM: molecules

1. Introduction

Planetary systems are formed in protoplanetary disks around young stars, while star-disk systems are formed by the gravitational collapse of precursor molecular clouds. The study of the evolution of molecular abundances in protoplanetary disks is important because it can reveal the chemical connection between planetary matter and interstellar matter, and eventually help determine from what material the bodies in planetary systems are made. The molecular composition in turn determines some of the basic properties of planets such as density, thermal history, and atmospheric composition. Knowledge of the molecular abundances at each radius of a disk is therefore helpful in understanding and predicting the properties of individual planets formed at different radii.

Recent radio observations are making great progress in the study of molecular abundances in protoplanetary disks. Emission lines of the CO molecule have been detected for T Tauri stars (Skrutskie et al. 1993; Guilloteau & Dutrey 1994; Handa et al. 1995), while aperture-synthesis images have directly revealed the distribution of CO around some T Tauri stars in the Taurus molecular cloud with a spatial resolution of a few hundred AU (Kawabe et al. 1993; Koerner et al. 1993; Dutrey et al. 1994; Koerner & Sargent 1995; Saito et al. 1995; Guilloteau & Dutrey 1998). In addition to the CO studies, Dutrey et al. (1997) have surveyed other molecular lines in the disks around DM Tau and GG Tau. These stars, with ages $1\ 10^6$ yr and $3\ 10^5$ yr respectively (Beckwith et al. 1990; Handa et al. 1995), have large gaseous disks with radii ~ 800 AU. Although the disk around GG Tau is, in fact, a circumbinary object, the physical conditions in the GG Tau disk seem similar to those in "normal" circumstellar disks. The molecular line spectra detected towards these two stars are similar. Dutrey et al. (1997) reported average fractional abundances of CO, CN, CS, HCN, HNC, H_2CO, C_2H, and HCO^+, and found that the abundances of these molecules are lower than those in molecular clouds by a factor of 10–100. These are the first observational data suggesting that molecular evolution occurs in protoplanetary disks. Such an interpretation of the abundances is controversial, however, and raises a variety of questions. What, for example, is the cause of the different molecular abundances in disks and clouds? Are the distributions of molecular abundances homogeneous throughout disks or significantly heterogeneous? Can we use detected molecular emission lines as indicators of physical conditions in disks? The answers to these and other questions require the use of detailed chemical models.

Send offprint requests to: Yuri Aikawa

In recent years, some theoretical work has already been undertaken on molecular evolution in protoplanetary disks. Chemical reactions in stationary disks including ion-molecule processes have been investigated by Aikawa et al. (1997). Molecular evolution in disks with accretion flows has been investigated by several authors (Finocchi & Gail 1997; Aikawa et al. 1998; Willacy et al. 1998; Aikawa et al. 1999). Among these authors, Aikawa et al. (1998; 1999) and Willacy et al. (1998) pointed out the importance of gas-dust interactions to the chemistry. In the outer region of disks ($R \gtrsim 10$ AU), many kinds of species deplete onto grain surfaces and form icy mantles because of the low temperature and high density. Aikawa et al. (1998; 1999) showed that the calculated composition of icy mantles is consistent with the molecular composition in comets.

These previous chemical modeling studies, however, consider only the midplane of the disk. Since there is a steep gradient of density in the direction perpendicular to the midplane, molecular abundances must be different away from the midplane, where the density is much lower. Aikawa et al. (1996) investigated the two-dimensional distribution of CO molecules in the disk. They found that at a typical age for the disk of 10^5–10^6 yr, significant amounts of CO remain in the gas phase in the surface (high Z) and intermediate regions, while CO is depleted onto grain mantles in the midplane. Since the observational data yield only the column densities of molecules, it is important to calculate not only molecular abundances in the midplane, but also the two-dimensional distribution (height and radial position) of molecules in the disk, so that we can compare theoretical models with observational data.

In this paper we calculate two-dimensional distributions and column densities for various molecules in a protoplanetary disk, and compare these with the observational data at radio wavelengths. The rest of the paper is organized as follows. In Sect. 2 we describe our model of a protoplanetary disk and the chemical reaction network we utilize. Numerical results on the evolution and distribution of molecular abundances, molecular column densities, and the dependence of these results on disk mass are shown in Sect. 3. In Sect. 4, we compare our results with the observational data, and discuss the effect of non-thermal desorption, dust sedimentation, and the mixing of matter by turbulence and accretion flow.

2. Model

2.1. Disk model

To date, much work has been undertaken to formulate the structure and physical evolution of protoplanetary disks (Cameron 1973; Hayashi 1981; Adams & Lin 1993, and references therein). In spite of these efforts it is still controversial which, if any, model can be adopted as the standard one. The main goal of this paper is to utilize detailed chemical modeling to investigate the two-dimensional distribution of molecules in a disk. Although it would be better if we could solve for molecular evolution together with physical evolution in the disk, such a calculation would be too complex at this time. In addition, it is useful, as a first step, to comprehend the essential characteristics of disk chemistry using a simple disk model, in which the physical conditions do not change with time. Hence we adopt one of the simplest models for the disk structure – the minimum-mass solar nebula of Hayashi (1981). We do, however, discuss the effects of variation in the disk model in a later section.

The minimum-mass solar nebula model is obtained by redistributing smoothly the matter of the present solar system so that the dust/gas mass ratio is 1%. In spite of its simple derivation, this model fits the observed continuum emission from disks at radio and infrared wavelengths fairy well (e.g. Beckwith et al. 1990). Although the original minimum-mass model extends only through a radius $R_{\rm out} = 36$ AU, we extend the model to an outer radius of about $R_{\rm out} \sim 10^3$ AU, and investigate the region of radius $100 \lesssim R \lesssim 800$ AU, because in a survey of gaseous disks around T Tauri stars, several disks were found to have outer radii at the upper limit. The radial distributions of column density of hydrogen nuclei $\Sigma_{\rm H}$ (cm^{-2}) and temperature (K) in the model are given by the equations

$$\Sigma_{\rm H}(R) \ = \ 7.2\ 10^{23} \left(\frac{R}{100{\rm AU}} \right)^{-3/2} \tag{1}$$

$$T(R) \ = \ 28 \left(\frac{R}{100{\rm AU}} \right)^{-1/2} \left(\frac{L_*}{L_\odot} \right)^{1/4} . \tag{2}$$

The luminosity of the central star L_* is assumed to be 1 $L_\odot$ in this paper. We adopt cylindrical coordinates (R, Ψ, Z) with the midplane of the nebula defined by $Z = 0$. Note that when discussing our chemical results, we also use the word "midplane" to refer to a range of heights from $Z = 0$ through roughly the height at which the density drops to $1/e$ of its $Z = 0$ value. It is assumed for simplicity that the disk is isothermal in the Z-direction and is cylindrically symmetric.

From the condition of hydrostatic equilibrium in the Z-direction with the mass distribution given by Eq. (1) and the temperature distribution given by Eq. (2), the density distribution by number of hydrogen nuclei (cm^{-3}) is given by the equation

$$n_{\rm H}(R,Z) \ = \ 1.9\ 10^9 \left(\frac{R}{100{\rm AU}} \right)^{-11/4} \exp\left(-\frac{GM_*\mu m_{\rm H}}{RkT} \right) \times \ \exp\left[\frac{GM_*\mu m_{\rm H}}{kT(R^2+Z^2)^{1/2}} \right] \tag{3}$$

where G is the gravitational constant, μ is the mean molecular weight of gas, $m_{\rm H}$ is the mass of a hydrogen atom, and k is the Boltzmann constant. We adopt $\mu = 2.37$ (Anders & Grevesse 1989) and $M_* = 1 M_\odot$ in this paper.

2.2. Reaction network

The basic equations for molecular evolution are given by

$$\frac{dn(i)}{dt} = \sum_j \alpha_{ij} n(j) + \sum_{j,k} \beta_{ijk} n(j) n(k), \tag{4}$$

where $n(i)$ is the number density of species i, and the α_{ij} and β_{ijk} are rate coefficients. The first term on the right-hand side

of Eq. (4) represents reactions with external particles such as ionization by cosmic rays. The second term represents two-body reactions in which species i are formed by the reactions of species j and k, or species i ($= j$) are destroyed by reactions with k.

We have adopted the so-called "new standard model" network of chemical reactions for the gas-phase chemistry (Terzieva & Herbst 1998; see also Osamura et al. 1999 for updated data). In addition to reactions in the gas phase, we also take into account the formation of H_2 molecules and the recombination of ions and electrons on grain surfaces. In the midplane of disks, especially at inner radii ($R \lesssim 100$ AU), which possess a higher density than a dense cloud core, recombination on grain surfaces is as important as that in the gas phase because ions collide with charged grains frequently. We assume that recombination reactions on grain surfaces are dissociative (Aikawa & Herbst 1999). The formation of ice mantles due to adsorption of gaseous molecules and the thermal desorption of molecules from ice mantles are explicitly followed. For simplicity and clarity, we do not consider other chemical reactions on grain surfaces because the reaction rates are still uncertain and because the whole concept of grain reaction rates is still controversial, especially at higher temperatures than in molecular clouds (Caselli et al. 1998; Shalabiea et al. 1998). For thermal desorption from ice mantles, we adopt the same rate coefficients as in Aikawa et al. (1997) (see also Yamamoto et al. 1983; Hasegawa & Herbst 1993; Sandford & Allamandola 1993). The total numbers of species and reactions included in our network are 577 and 4601, respectively.

For elemental abundances, we assume the so-called "low-metal" values (e.g. Lee et al. 1998; Aikawa et al. 1999). The initial molecular abundances used in the disk chemistry are determined by following molecular evolution in a precursor molecular cloud core with physical conditions $n_{\rm H} = 2\ 10^4\,{\rm cm}^{-3}$ and $T = 10\,{\rm K}$ up to $3\ 10^5$ yr, at which time we can reproduce observed molecular abundances in cloud cores fairly well (Terzieva & Herbst 1998).

2.3. Sticking probability

The efficiency of adsorption and desorption of molecules onto and from grain surfaces is a controversial subject. The adsorption rate is equal to the sticking probability times the collision rate between a gaseous molecule and a grain particle. In the low temperature regime, the sticking probability is estimated to be 0.3–1.0 (Williams 1993; and references therein). The story is more complicated for desorption; in addition to desorption by thermal energy (evaporation), many non-thermal desorptions have been proposed, such as impulsive heating by cosmic rays (Léger, Jura & Omont 1985; Hasegawa & Herbst 1993) and chemical explosions (d'Hendecourt et al. 1982). Although semi-quantitative estimates of these rates are available, they depend on many parameters such as the intensity of radiation, and the morphology and size of grain particles. Instead of taking into account these detailed factors, we slow down the rate of adsorption by adopting a low effective sticking probability (Ruffle et al. 1997).

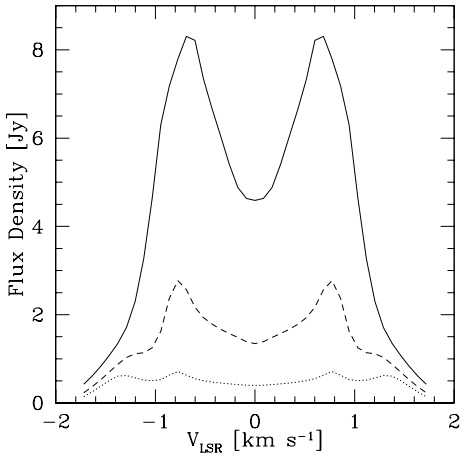

Fig. 1. Calculated rotational (J=2-1) line profiles of ^{12}CO (solid line), ^{13}CO (dashed line) and C^{18}O (dotted line) from the minimum-mass solar nebula model. The physical parameters are adopted from the observation of GG Tau; the outer radius $R_{\rm out}$=750 AU, inclination $i = 45^\circ$, the age $t = 3\ 10^5$ yr, and the distance from the earth $D = 140$ pc. The isotopic ratios for ^{12}C/^{13}C and ^{18}O/^{16}O are assumed to be 60 and 570, respectively.

We estimate the effective sticking probability from the intensity of the CO emission lines observed towards GG Tau. According to Aikawa et al. (1996), the column density of gaseous CO at $R \gtrsim 200$ AU depends mainly on the sticking probability and age of the disk, and does not depend significantly on other parameters such as the mass of the disk. The lack of dependence on disk mass stems from the fact that gaseous CO is found mainly in intermediate and surface regions rather than in the disk midplane, where the CO is mainly depleted onto grain surfaces, and it is the density of the midplane that is mainly affected by a change in disk mass. Although X-ray and UV radiation are not included in the model of Aikawa et al. (1996), the calculated CO abundance is not affected by either of these sources of radiation (see below).

Following Aikawa et al. (1996), we calculated the CO $J = 2 \rightarrow 1$ emission line for three isotopomers assuming various values of the sticking probability and found that the case with S=0.03 shows best reasonable agreement with the observed spectra for GG Tau. Our simulated emission features are shown in Fig. 1 while the actual observed line profiles are depicted in Dutrey et al. (1994); the peak values of the flux density are about 8–10 Jy, 2.5 Jy, and 0.4–0.5 Jy for ^{12}CO, ^{13}CO, and C^{18}O, respectively. We discuss the sticking probability and desorption mechanisms in more detail in Sect. 4.2.

2.4. Ionization rate

There are two main ionization sources in the disk: X-rays and cosmic rays. The X-ray observation satellites, ROSAT and ASCA, have found that the X-ray luminosity of T Tauri stars is in the range $10^{29} - 10^{31}$ erg s^{-1} (Montmerle et al. 1993; Glassgold

et al. 1997). Because X-rays irradiate the disk obliquely from the central star and because the attenuation length of X-rays is rather small ($10^{21} - 10^{23}\,\mathrm{cm}^{-2}$), ionization by X-rays is only effective in the regions removed from the midplane (Glassgold et al. 1997). On the other hand, cosmic rays are the main ionization source in the midplane, because the attenuation length of cosmic rays ($4\ 10^{25}\,\mathrm{cm}^{-2}$) is much larger than the column density at radii in the outer regions of disks ($R \gtrsim 100$ AU) with which we are concerned (Umebayashi & Nakano 1981). For the ionization rate by cosmic rays, $\zeta_{\rm CR}$, we adopt the standard value of $1.3\ 10^{-17}\,\mathrm{s}^{-1}$.

The ionization rate caused by X-rays, $\zeta_{\rm x}$, obtained following Maloney et al. (1996) and Glassgold et al. (1997), is given by

$$\zeta_{\rm x} = N_{\rm sec} \int_{1{\rm keV}}^{30{\rm keV}} \sigma(E) F(E) dE, \quad (5)$$

where $N_{\rm sec}$ is the number of secondary ionizations per unit photoelectron energy, and the photon flux $F(E)$ is given by

$$F(E) = F_{\rm o}(E) e^{-\tau(E)}, \quad (6)$$

where $\tau(E)$ is the optical depth corresponding to the column density between the central star and the point in question. This column density is discussed further below (see Sect. 2.5). We assume that the X-ray spectrum is thermal with characteristic temperature 5 keV (Koyama et al. 1994; Glassgold et al. 1997). The cross section for X-ray absorption per hydrogen nucleus is expressed by the relations

$$\sigma(E) \ = \ 2.6\ 10^{-22} E^{-8/3}\ \mathrm{cm}^2 \ \text{for}\ 1{\rm keV} \le E \le 7{\rm keV} \quad (7)$$

$$\sigma(E) \ = \ 4.4\ 10^{-22} E^{-8/3}\ \mathrm{cm}^2 \ \text{for}\ 7{\rm keV} < E. \quad (8)$$

Scattering is not important, because the optical depth for the Thomson scattering is smaller than unity in outer regions of disks (Glassgold 1999, personal communication).

The total ionization rate ζ ($= \zeta_{\rm X} + \zeta_{\rm CR}$) at $R = 700$ AU is plotted versus height Z at R = 700 AU in Fig. 2 for different X-ray luminosities. At inner radii, the total ionization rate shows similar dependence on the height Z, but the value at the surface region is higher because of the shorter distance from the central star. It can be seen that X-rays enhance the value of ζ significantly at high Z especially if the luminosity is near its maximum value of $L_{\rm X} = 1\ 10^{31}\,\mathrm{erg\,s}^{-1}$. For the case of $L_{\rm X} = 1\ 10^{28}\,\mathrm{erg\,s}^{-1}$, on the other hand, the ionization rate is close to the value which is determined by cosmic rays at all heights. Considering the variation of the X-ray luminosity from T Tauri stars, we calculate molecular abundances for two cases: (1) $L_{\rm X} = 1\ 10^{31}\,\mathrm{erg\,s}^{-1}$ (corresponding to the uppermost curve in Fig. 2), and (2) $\zeta = 1.3\ 10^{-17}\,\mathrm{s}^{-1}$ throughout the disk.

In addition to the ionization, our model includes photoprocesses caused by the UV radiation induced by cosmic rays and X-rays (Gredel et al. 1989; Maloney et al. 1996).

2.5. UV radiation

The protoplanetary disk is irradiated by UV radiation from both the interstellar field and the central star, which causes ionization and dissociation of molecules. In analogy with cosmic rays and X-rays, the radiation from these two sources strikes the disk from different directions, as shown in Fig. 3. The UV flux from the central star varies, and can be as high as 10^4 times as strong as the interstellar flux at $R = 100$ AU (Herbig & Goodrich 1986; Imhoff & Appenzeller 1987; Montmerle et al. 1993). In this paper we assume this highest value hereinafter. We have calculated the UV flux at various radii in the disk as a function of height Z, and show the results in Fig. 4. The flux is expressed relative to the average interstellar UV flux ($\equiv 1G_o$). Note that for the calculation, we assumed the UV radiation to lie at 1000 Å or, alternately, to have an extinction of unity for a column density of $5\ 10^{20}\,\mathrm{cm}^{-2}$. In case the stellar UV flux is smaller by an order of magnitude than assumed here, the flux at the extreme surface region (e.g. $Z \gtrsim 400$ AU for R=700 AU) is smaller by the same factor. The height at which the reduced UV flux is $1G_o$ does not change significantly.

Although the UV radiation is mainly attenuated by dust, self- and mutual-shielding are important for H_2 and CO (van Dishoeck & Black 1988; Lee et al. 1996). For these molecules,

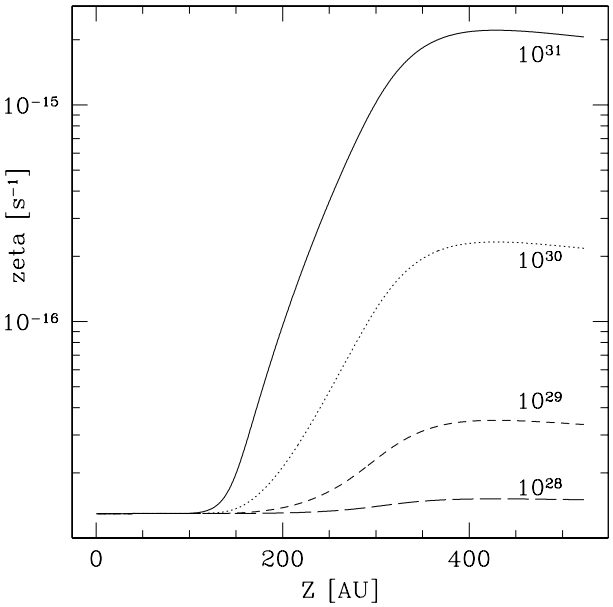

Fig. 2. The total ionization rate ζ (s^{-1}) at $R = 700$ AU as a function of height Z. The numbers next to each curve indicate the X-ray luminosity from the central star in units of $\mathrm{erg\,s}^{-1}$.

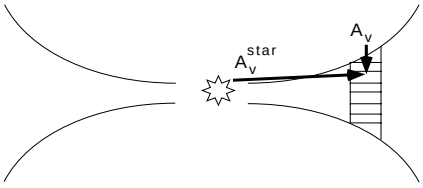

Fig. 3. Schematic figure for the disk model showing as outer boundaries the flaring of the height at which the UV radiation field is $1G_o$. Regions of the disk defined by a specific radius are horizontally separated into several slabs in which radiative transfer from the interstellar radiation field and molecular evolution are calculated self-consistently.

we have to solve for the molecular abundances and the UV attenuation self-consistently. In this paper, we adopt a one-dimensional slab model, as described in Lee et al. (1996), and shown schematically in Fig. 3. We separate a local region of the disk at radius R into several layers, or slabs, depending on height Z, and calculate the molecular abundances in each layer. We begin each calculation at a height with a UV flux $\sim 1G_o$. We neglect higher regions (with greater UV flux), because most of the gas in these regions consists of atoms and ions, owing to the low density and high UV flux there. Below this upper height limit, we calculate molecular abundances by including UV radiation both from the interstellar field and the central star, and by considering extinction by grain particles and molecular lines. The interstellar radiation strikes each portion of the disk from above. Given the one-dimensional nature of our slab treatment, we assume for simplicity that CO and H_2 are shielded from the *stellar* UV because a proper radiative transfer treatment of radiation emanating from the central star would require us to solve for the radiative transfer and distribution of molecules in two dimensions (R, Z) at the same time, which is too complicated. Since the stellar UV is effective only within a very thin surface layer, where the density is the lowest, this simplification does not much affect our results.

The shielding factor for interstellar UV radiation for the dissociation of CO and H_2 is given as a function of H_2 column density, CO column density, and A_v (Lee et al. 1996). In the observation of CO emission towards the DM Tau disk, the local velocity dispersion in the disk is found to be essentially thermal (Guilloteau & Dutrey 1998). Since the thermal line widths in the outer region of the disk are much smaller than the turbulent line width (3 km s^{-1} in Doppler velocity units) adopted in Lee et al. (1996), we multiplied the H_2 column density in Table 10 of Lee et al. (1996) by C_s/(3 km s^{-1}), where C_s is the sound velocity, in calculating the shielding factor for H_2. This re-normalization is not used for CO shielding, because the widths of CO dissociation lines are intrinsically very large ($\gtrsim$ a few km s^{-1}) due to predissociation.

3. Results

3.1. Evolution at each height

At each point in the disk, physical conditions are given as described above, and the molecular evolution is obtained by solving Eqs. (4). We neglect hydrodynamic evolution and mixing of matter for simplicity. These effects are discussed in Sect. 4.

As an example, we consider molecular evolution at $R = 700$ AU, because this outer region of the disk contributes significantly to the molecular emission lines owing to its large area. The fixed temperature of $T = 10.58$ K for this region comes from Eq. (2). The slab grid and physical conditions at each height are given for $R = 700$ AU in Table 1. The density n_H varies from $2\ 10^5$ cm^{-3} to $9\ 10^6$ cm^{-3}, while the ionization rate ζ varies from $1.3\ 10^{-17}$ s^{-1} to $2\ 10^{-15}$ s^{-1} as a function of height for the case in which we include ionization by X-rays. The fourth column shows the continuum extinction of interstellar radiation A_v and the last column shows the extinction of the radiation from the central star A_v^{star} (Fig. 3). The unextinguished UV flux from the central star is about 160 times larger than the interstellar UV at this radius. We assume no extinction by any remnant of the parent molecular cloud core.

Figs. 5a, b, and c show the calculated molecular evolution in the disk for assorted species at $R = 700$ AU and heights Z of

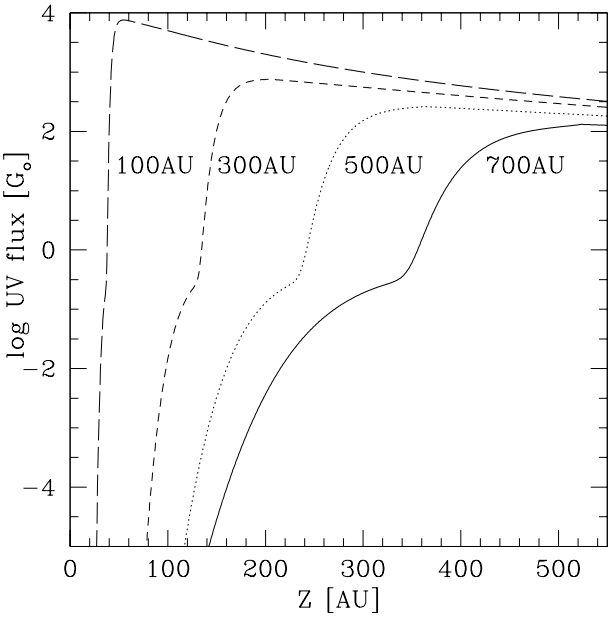

Fig. 4. The UV flux at various radii in the disk as a function of height Z. The flux is normalized to the average UV flux in interstellar field ($\equiv 1G_o$).

Table 1. Physical parameters of the slab model at R = 700 AU

Z [AU]	n_H [cm^{-3}]	ζ [s^{-1}]	A_v [mag]	A_v^{star} [mag]
360	2.039(5)	1.945(-15)	9.046(-2)	1.350
355	2.227(5)	1.893(-15)	9.916(-2)	1.529
350	2.430(5)	1.836(-15)	1.087(-1)	1.732
345	2.651(5)	1.773(-15)	1.190(-1)	1.963
340	2.891(5)	1.705(-15)	1.303(-1)	2.227
330	3.431(5)	1.553(-15)	1.561(-1)	2.872
320	4.062(5)	1.384(-15)	1.866(-1)	3.715
310	4.797(5)	1.205(-15)	2.227(-1)	4.820
300	5.650(5)	1.025(-15)	2.653(-1)	6.278
280	7.770(5)	6.996(-16)	3.740(-1)	1.079(1)
260	1.055(6)	4.525(-16)	5.225(-1)	1.892(1)
240	1.410(6)	2.816(-16)	7.225(-1)	3.409(1)
220	1.856(6)	1.682(-16)	9.877(-1)	6.358(1)
200	2.400(6)	9.583(-17)	1.334	1.241(2)
180	3.045(6)	5.163(-17)	1.776	2.571(2)
160	3.784(6)	2.667(-17)	2.332	5.762(2)
140	4.600(6)	1.606(-17)	3.014	1.434(3)
120	5.464(6)	1.347(-17)	3.834	4.117(3)
100	6.334(6)	1.303(-17)	4.795	...
80	7.158(6)	1.300(-17)	5.895	...
60	7.880(6)	1.300(-17)	7.121	...
40	8.443(6)	1.300(-17)	8.451	...
20	8.803(6)	1.301(-17)	9.857	...

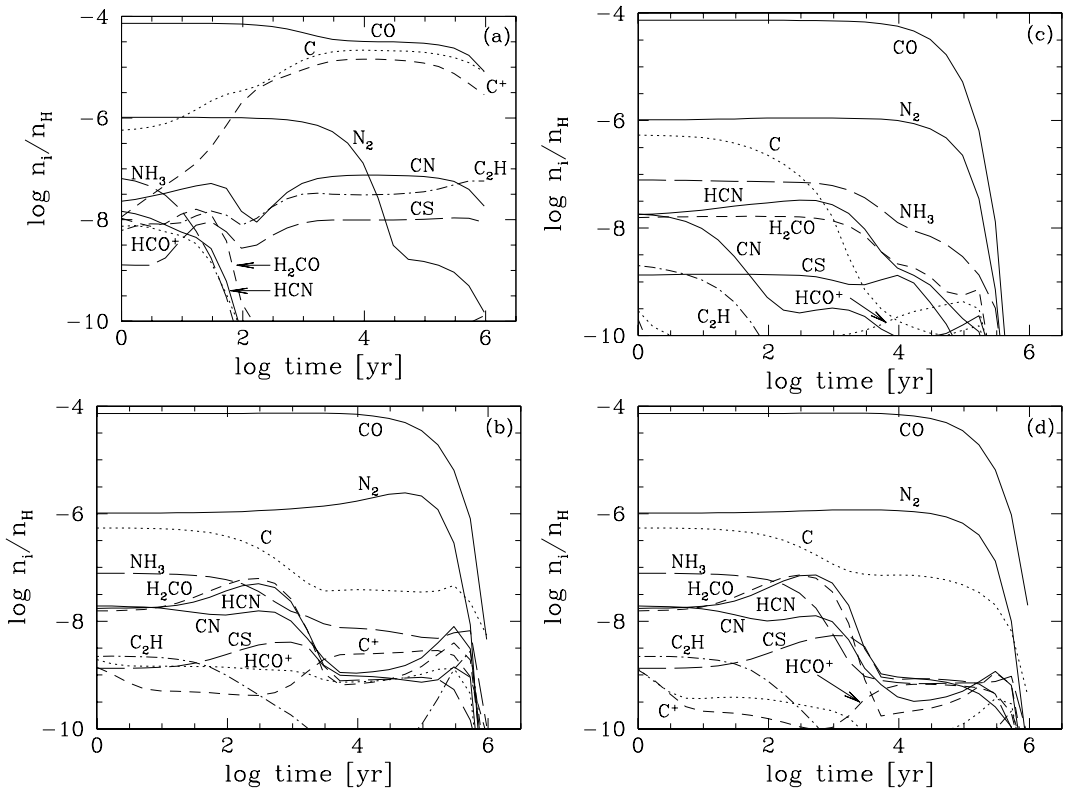

Fig. 5a–d. Temporal evolution of molecular abundances at $R = 700$ AU and heights Z of 350 AU **a**, 220 AU **b**, and 100 AU **c**. The ionization rate is enhanced by X-ray emission from the central star ($L_{\rm x} = 1\ 10^{31}$ erg s^{-1}). **d** shows the molecular evolution at a height of 220 AU, but with a lower ionization rate $1.3\ 10^{-17}$ s^{-1} produced solely by cosmic rays.

350 AU, 220 AU, and 100 AU, respectively, and the maximum ionization rate including X-rays. Fig. 5d shows the molecular evolution at $Z = 220$ AU, but with the lower ionization rate $\zeta = 1.3\ 10^{-17}$ s^{-1} caused solely by cosmic rays. The plotted abundances are normalized by the number density of hydrogen nuclei, $n_{\rm H}$. At $Z = 350$ AU, the molecular abundances are similar to those of a photodissociation region; atoms, ions, and radicals such as C_2H and CN are abundant. Many gas-phase species reach a quasi-steady state abundance by 10^4 yr, although abundances tend to decrease by $t = 10^6$ yr due to adsorption onto grains. At $Z = 220$ AU, the UV radiation is partially attenuated and molecules such as HCN and NH_3 can retain a significant portion of their initial abundance until adsorption onto dust grains occurs. The secondary peak at late times shown for some molecules is reminiscent of that found for HC_3N in evolved cores by Ruffle et al. (1997). At $Z = 100$ AU, most molecules containing heavy elements deplete onto grains before 10^6 yr, because of the higher gas and dust density. The effect of X-rays can be seen by comparing Fig. 5b and d. Other than CO and N_2, the molecules shown tend to be more abundant at times between 10^4 yr and 10^6 yr in the case with X-ray ionization by a factor of 3–10, because formation of these molecules is aided by the increasing abundances of assorted ions.

3.2. Vertical distribution

Fig. 6 shows the vertical distribution of various kinds of molecules at $R = 700$ AU and at $t = 3\ 10^5$ yr, which is a typical age of a T Tauri star. The solid lines are for the case in which X-rays are included, while the dotted lines are for the other case. At the midplane, most of the molecules are adsorbed onto grains by the time depicted owing to the high density. At or near the surface, molecules tend to be dissociated by UV radiation. Hence the molecular abundances have their peak values at some intermediate region. The height at which a given molecular abundance reaches its peak value varies with species. Radicals, such as CN and C_2H, have their peak abundances at larger heights Z compared with more stable species such as HCN and NH_3. The abundances of most molecules are higher when X-rays are included, as described in the previous subsection.

The gradients in the abundances of CO, CN, and C_2H at $Z = 355$ AU seem too abrupt. They are partially caused by the choice of an outer boundary of $Z = 360$ AU in our calculation. If we begin the integration at a larger height (e.g. $Z = 400$ AU), the slopes are less steep. The total column densities, however, are not much affected since the density is smaller at these upper regions.

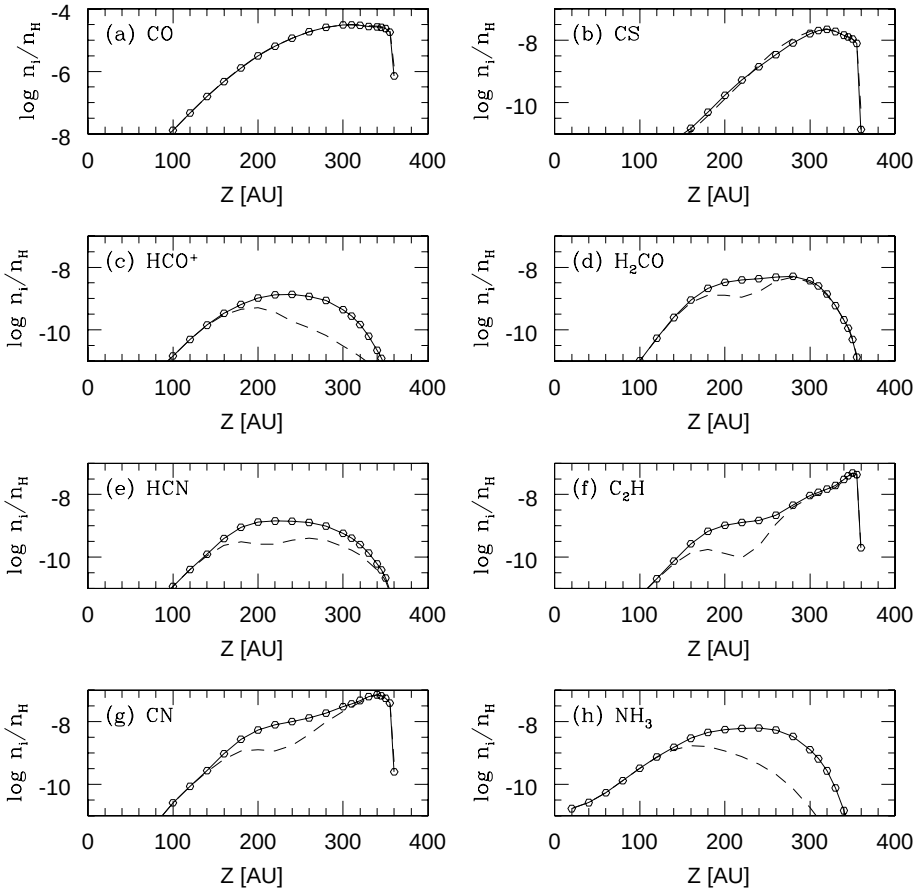

Fig. 6a–h. Vertical distribution of molecules at $R = 700$ AU and $t = 3\ 10^5$ yr. The solid lines with open circles show the results of a model in which ionization by X-rays from the central star is included. The dashed lines show the results of a model without the enhanced ionization rate.

3.3. Column densities

By integrating the vertical distributions of molecular abundances, we obtain molecular column densities as a function of disk radius. Fig. 7 shows selected radial distributions of molecular column densities for assorted molecules. The thick lines show the column densities at $t = 3\ 10^5$ yr, and the thin lines at $t = 9.5\ 10^5$ yr. Solid lines show the case with the higher ionization rate, while dashed lines show the case with the lower ionization rate.

At radii greater than 300 AU, the column density of gas-phase CO is almost independent of radius, with only a weak increase with increasing radius. At these radii, gaseous CO exists only in regions removed from the midplane, and the amount of gas contained in these regions weakly increases with increasing radius, because the disk is more compressed by stellar gravity at smaller radii. At a radius near 200 AU, however, the temperature warms to the sublimation temperature of CO ($T \sim 20$ K). Hence the column density of gas-phase CO becomes much higher at $R \lesssim 200$ AU (Aikawa et al. 1996). The calculated radial distribution of HCO^+ is similar to that of CO, since it is formed directly from CO via the reaction with H_3^+. The gradient at $R \sim 200$ AU is shallower than that of CO, because of a lower degree of ionization at smaller radii due to higher densities. The radial distributions of other carbon-bearing molecules also weakly increase with increasing radius beyond 300 AU, for the same reason as for CO, and because CO is a precursor of most of these species (viz. through the reaction of CO with He^+). The small bump that the column densities of the carbon-bearing molecules show at or near $R \sim 200$ AU is caused by the desorption of CO. Since ammonia is formed from N_2, its distribution is different from carbon-bearing molecules formed from CO. The sublimation temperature of N_2 is about 17 K, and this value occurs at a large radius of around 300 AU rather than at 200 AU as for the sublimation of CO.

Comparing the thick lines ($t = 3\ 10^5$ yr) and thin lines ($t = 9.5\ 10^5$ yr) in Fig. 7, we can see the time variation of the molecular column densities. Due to adsorption onto grains, the molecular column densities decrease with time in the outer region, where the temperature is lower than the sublimation temperature of CO or N_2 (see also Sect. 4.2).

Table 2 shows the column densities of a wide assortment of species in the gas phase at $R = 700$ AU and $t = 3\ 10^5$ yr. Only those species with column densities larger than 10^{12} cm^{-2} are listed, except for N_2H^+, which was detected by Dutrey et al. (1997). We can see that CO, CN, CS, and H_2CO, also detected by Dutrey et al. (1997), are indeed among the more abundant molecules. Certain carbon-chain molecules and hydrocarbons are also surprisingly abundant. For example, C_5 has a large column density at R = 700 AU approaching 10^{14} cm^{-2}. The vertical distribution of this species peaks strongly in the surface regions, where the UV radiation is high. The surprising abundance of carbon chain molecules for dense photon-dominated regions was first discussed by Suzuki (1983). Since our radia-

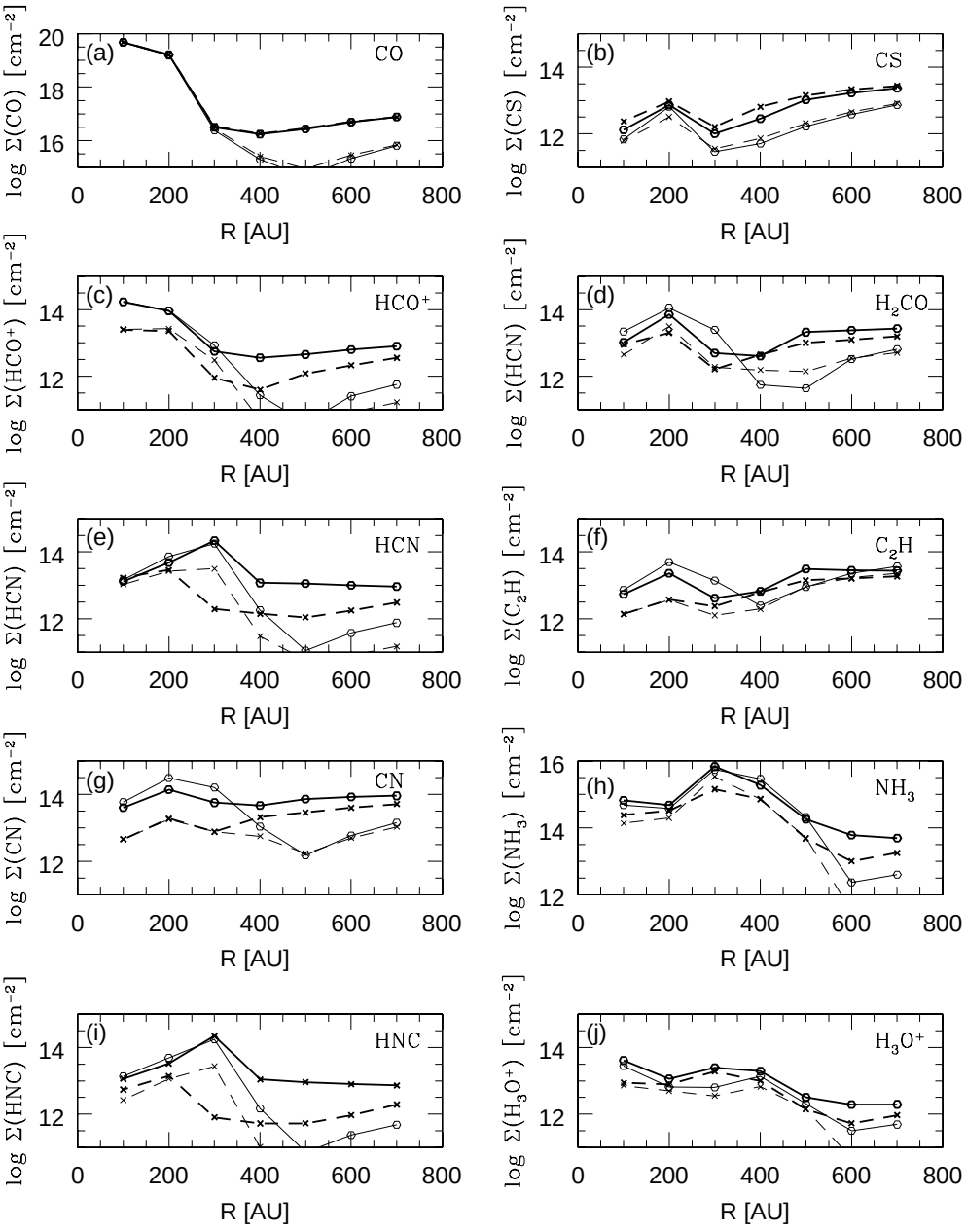

Fig. 7a–j. Radial distribution of molecular column densities. The solid lines are for the model with the higher ionization rate while the dashed lines show the model with the lower ionization rate. The thick lines show the column densities at $t = 3\ 10^5$ yr, and thin lines at $9.5\ 10^5$ yr.

tive transfer treatment of H_2 is approximate in these regions, one must treat this result carefully. Overall, there appear to be many molecules suitable for detection.

3.4. Dependence on disk mass

In the model results discussed in the previous subsections, we utilized the minimum-mass solar nebula model extended to an outer radius of several hundred AU. Although this model fits many observed disk parameters (Beckwith et al. 1990), mass varies for individual objects. According to Dutrey et al. (1994) and Dutrey et al. (1997), the best models of the extended disks around GG Tau and DM Tau are, in fact, less massive than the minimum-mass model by a factor of ~ 10.

To compare our model results with the observations of GG Tau and DM Tau, we adopt a disk model less massive than the minimum-mass model by a factor of 10. The temperature distribution and the functional dependence of the density distribution are the same as in Eqs. (2) and (3), respectively. The fourth column of Table 2 lists assorted molecular column densities at $R = 700$ AU and at $t = 3\ 10^5$ yr using the less massive disk model, while Fig. 8 shows the radial distributions of selected molecular column densities at $t = 3\ 10^5$ yr. The column densities of HNC, NH_3, HCO^+, and H_3O^+ are quite noticeably affected by the change in mass, becoming smaller by a factor of > 10 at regions of radius $R \gtrsim 500$ AU compared with the minimum-mass disk model. In the less massive disk, where the shielding of UV radiation is less effective, these molecules are destroyed more efficiently. Since these species are especially

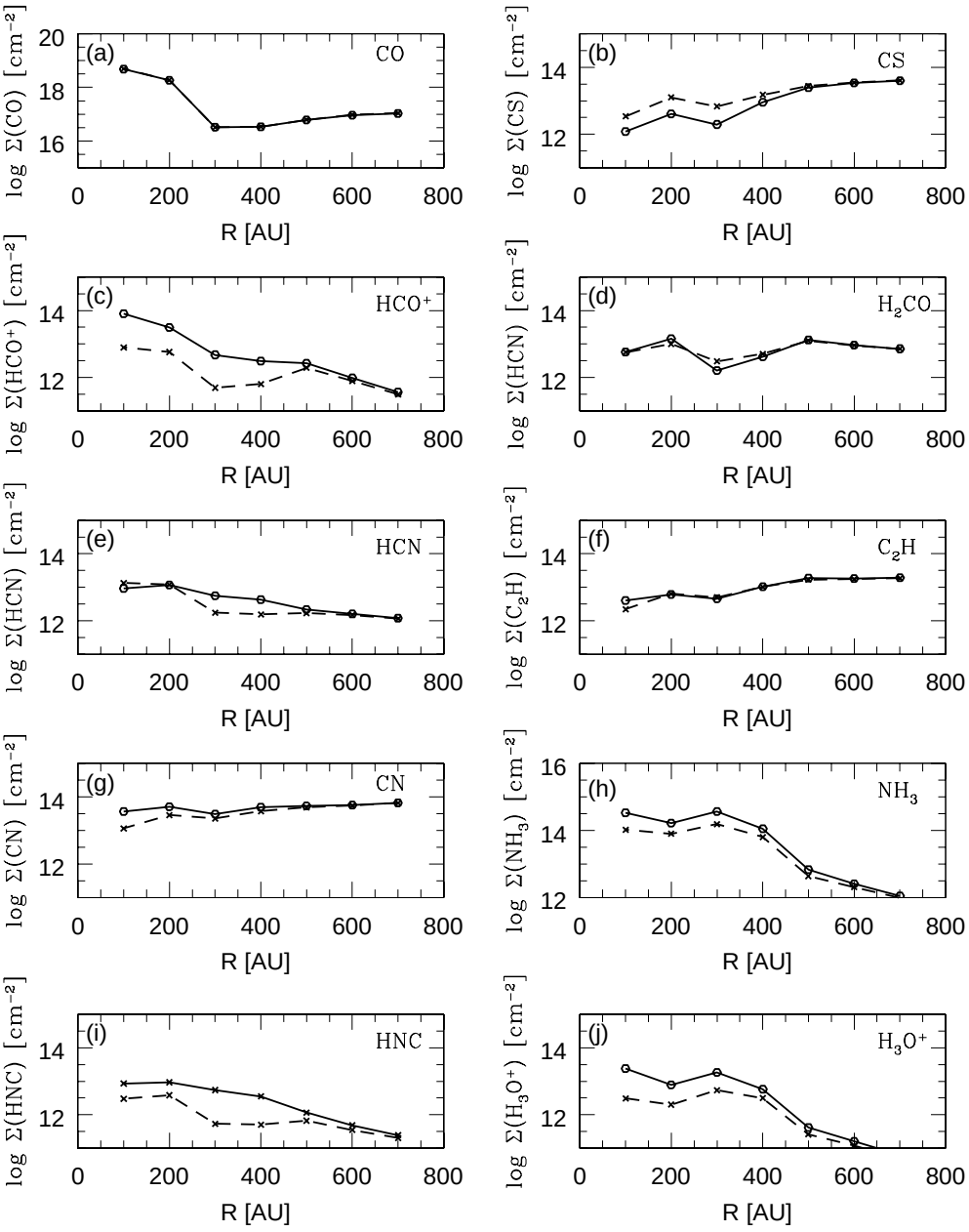

Fig. 8a–j. Radial distribution of molecular column densities at $t = 3\ 10^5$ yr. The disk mass is smaller than the "minimum-mass" disk by an order of magnitude. Other details are the same as in Fig. 7.

sensitive to disk mass, they can be used as probes to estimate the total column density of the disk. The column density of CO at radii $R \gtrsim 300$ AU does not depend on the disk mass, because CO is shielded from UV radiation efficiently by lines of H_2 and CO itself. On the other hand, the column densities of radicals, such as CN and C_2H, do not show much dependence on the disk model, because they are abundant at the disk surface, where photolysis dominates the chemistry.

4. Discussion

4.1. Comparison with observational data

Table 3 shows the molecular abundances relative to H_2 in the DM Tau disk estimated from the observational data by Dutrey et al. (1997), who assumed that the relative abundances are constant throughout the disk. In Fig. 9 we show the averaged fractional abundances using our less massive disk model obtained by dividing the molecular column densities by the column density of H_2 at each radius. As previously, the solid lines show the model with higher ionization rate, the dashed lines are for the model with the lower ionization rate, the thick lines are for $t = 3\ 10^5$ yr, and thin lines for $9.5\ 10^5$ yr. The dotted lines show the averaged abundances obtained by Dutrey et al. (1997). Considering that the age of DM Tau is $1\ 10^6$ yr, and that the observational data are more sensitive to the outer regions, we can see reasonable agreement for CO, CN, HCO^+, HCN, HNC, and C_2H, where the differences between the model results and the estimated values from the observational data differ only by a factor of a few. The abundances of CS and H_2CO disagree, on the other hand, by a factor of 10–30.

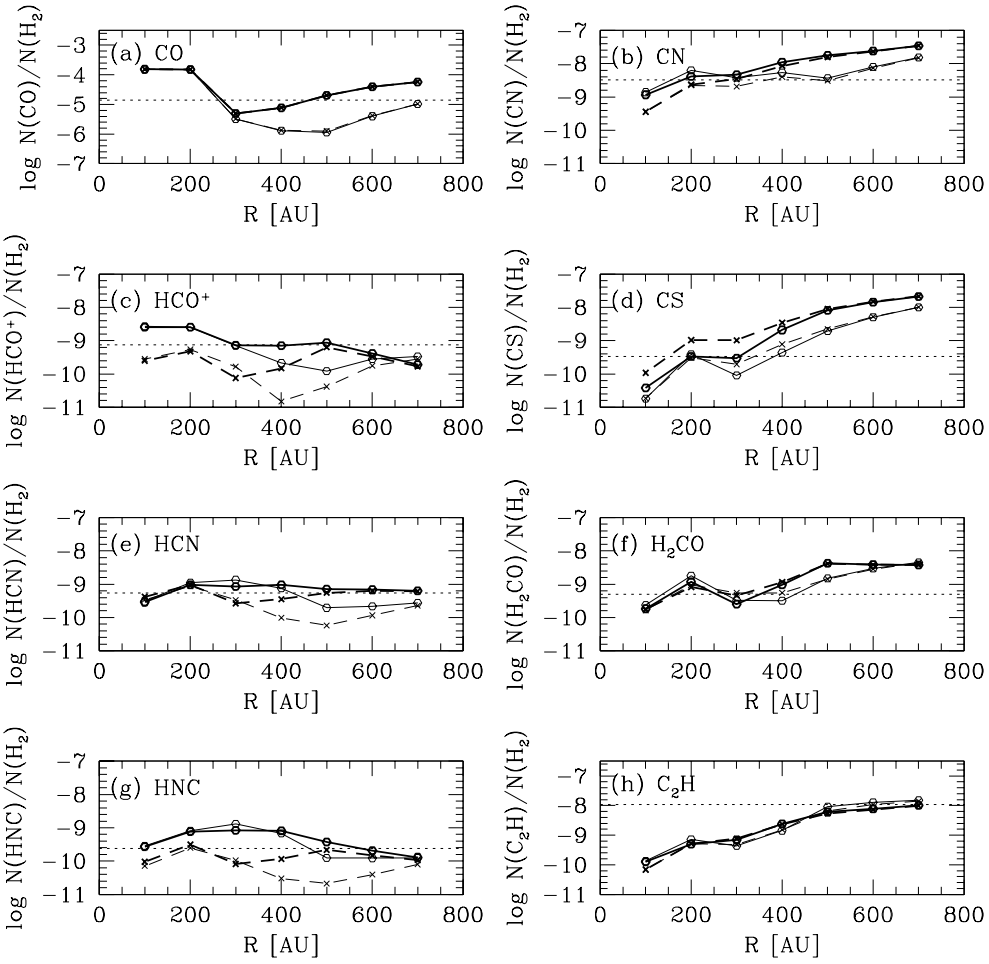

Fig. 9a–h. The averaged molecular abundances relative to H_2. Other details are the same as in Fig. 7.

The discrepancies for CS and for H_2CO may be caused by several factors. First, there may be errors caused by uncertainties in reaction rates. Formaldehyde (H_2CO) is formed mainly by the reaction of O atoms with CH_3. In our model there is no activation energy for this reaction. Since the reaction has only been studied down to room temperature, there is always the possibility for a small activation energy barrier. Another possible source of error in our model is the somewhat arbitrary choice of initial conditions. The abundance of atomic O in the gas phase depends on its initial abundance. Initial abundances are determined by calculating molecular evolution in the molecular cloud state ($n_{\rm H} = 2\ 10^4\ {\rm cm}^{-3}$, $T = 10\,{\rm K}$) up to $3\ 10^5$ yr. If we assume a longer time scale for the cloud phase, more oxygen will be transformed into molecules such as water and deplete onto grains, which will eventually result in a lowered abundance for H_2CO in the disk. Similarly, the abundance of CS is dependent on the initial elemental abundance of sulfur. The amount of gas-phase sulfur is uncertain even in the molecular cloud phase (Ruffle et al. 1999). Finally, there are uncertainties in the abundances estimated from the observational data. Dutrey et al. (1997) assumed constant abundance ratios throughout the disk, which is not entirely consistent with our theoretical model.

4.2. Sticking probability and non-thermal desorption

In this paper we adopt a sticking probability $S = 0.03$, which is chosen by fitting the observed spectrum of CO emission lines with an adsorption model. Since the value of S is much smaller than the range 0.3–1.0 estimated from the calculation of sticking processes (Williams 1993, and references therein), there must be some mechanism for non-thermal desorption in the disk. Although many mechanisms for non-thermal desorption have been discussed (Léger et al. 1985; d'Hendecourt et al. 1982; Willacy & Millar 1998; and references therein) to date, quantitative estimates of the desorption rates still contain significant uncertainties. Thus we must discuss the effects of non-thermal desorption on our results rather qualitatively.

Let us first look at the time scale $\tau_{\rm ads}$ (yr) for adsorption of CO, which is given by the equation

$$\tau_{\rm ads} = \frac{1}{\pi a^2 n({\rm grain}) S}\left[\frac{\pi m({\rm CO})}{8kT}\right]^{1/2} = 3\ 10^5 \left(\frac{7.8\ 10^4 {\rm cm}^{-3}}{n_{\rm H}}\right)\left(\frac{0.3}{S}\right)\left(\frac{10{\rm K}}{T}\right)^{1/2}, \quad (9)$$

where a is the radius of dust particles (assumed to be 0.1 μm), and m(CO) is the mass of CO. If one chooses S to be 0.3,

Table 2. Column densities (cm^{-2}) of assorted molecules at $R = 700$ AU and $t = 3\ 10^5$ yr.

Species	High Ionization	Low Ionization	Lower Mass	Sedimentation
C_2	6.5(14)	5.8(14)	8.7(14)	1.4(15)
CH	3.1(13)	2.6(13)	2.8(13)	7.2(13)
CN	9.1(13)	5.1(13)	6.6(13)	1.5(13)
CO	7.5(16)	7.6(16)	1.1(17)	5.3(16)
CS	2.3(13)	2.7(13)	4.0(13)	2.1(13)
H_2	1.9(22)	1.9(22)	1.9(21)	1.9(22)
N_2	1.4(15)	6.4(14)	4.6(14)	3.9(12)
NH	2.2(12)	6.6(11)	1.8(11)	2.4(11)
NO	4.5(13)	1.2(13)	3.3(12)	6.0(11)
O_2	5.7(14)	2.1(14)	2.5(13)	6.8(12)
OH	4.7(13)	2.6(13)	9.3(11)	5.5(12)
SiH	1.7(12)	2.1(12)	1.9(12)	3.3(12)
SiO	5.9(11)	1.4(12)	2.2(12)	4.0(11)
SO	3.2(11)	1.4(12)	1.5(12)	7.2(11)
C_2H	2.6(13)	1.8(13)	1.9(13)	4.2(13)
C_3	1.4(14)	1.2(14)	2.1(14)	1.4(14)
CH_2	1.4(14)	1.0(14)	9.5(13)	1.3(14)
CO_2	4.6(13)	2.7(13)	1.3(12)	2.4(11)
H_2O	1.0(14)	4.5(13)	7.4(12)	6.2(12)
HCN	9.3(12)	3.1(12)	1.2(12)	5.1(11)
HCO	2.1(12)	1.1(12)	3.0(11)	4.3(11)
HNC	7.3(12)	1.9(12)	2.5(11)	1.1(11)
HNO	2.5(12)	7.8(11)	5.1(11)	2.5(10)
NH_2	2.8(13)	9.5(12)	1.1(12)	1.3(12)
OCN	4.0(13)	2.1(13)	1.8(11)	2.7(10)
C_2H_2	3.3(13)	1.5(13)	1.2(13)	1.2(13)
C_3H	3.4(12)	2.4(12)	2.4(12)	2.5(12)
C_4	6.0(13)	5.1(13)	8.6(13)	2.1(13)
CH_3	1.2(14)	7.9(13)	1.4(13)	1.8(14)
H_2CN	2.4(12)	2.3(12)	1.5(12)	2.2(12)
H_2CO	2.7(13)	1.6(13)	7.2(12)	1.3(13)
NH_3	5.0(13)	1.8(13)	1.1(12)	1.2(12)
C_2H_3	4.2(12)	2.0(12)	1.4(12)	3.1(12)
C_3H_2	2.6(12)	1.8(12)	2.1(12)	1.6(12)
C_4H	6.8(12)	5.4(12)	9.4(12)	1.8(12)
C_5	6.3(13)	5.7(13)	1.2(14)	2.3(13)
CH_4	1.8(14)	1.1(14)	3.4(13)	3.8(13)
H_3^+	3.3(13)	2.4(13)	6.8(11)	1.5(13)
HCO^+	8.1(12)	3.6(12)	3.6(11)	7.9(11)
H_3O^+	2.0(12)	9.4(11)	6.3(10)	1.9(11)
N_2H^+	9.8(10)	3.8(10)	4.6(8)	5.8(7)

Table 3. Averaged molecular abundances in the DM Tau disk[a]

Species	Averaged Abundance
CO	1.4(-5)
CN	3.2(-9)
CS	3.3(-10)
C_2H	1.1(-8)
HCN	5.5(-10)
HNC	2.4(-10)
H_2CO	5.0(-10)
HCO^+	7.4(-10)

[a] From Dutrey et al. (1997).

then CO begins to be seriously depleted from the gas at the preferred lifetime of our disk ($3\ 10^5$ yr) for gas densities over $7.8\ 10^4\ cm^{-3}$. Even the surface region lies at densities above this value, and we achieve better agreement with CO observations if we lower the sticking coefficient by a factor of 10 ($S \sim 0.03$) so that effective depletion occurs only at a density $10\times$ larger. Lowering the sticking coefficient in this manner is equivalent to adding a desorption term that is proportional to the gas density of the adsorbing/desorbing molecule. Desorption is thus equally efficient per molecule at low and at high densities.

Mechanisms for non-thermal desorption can be divided into two groups. The first group of desorption mechanisms is caused by internal processes, such as exothermic chemical reactions on grain surfaces. In this case, the desorption rate is formally dependent on the density (e.g., a higher gaseous atomic hydrogen density leads to more hydrogen atoms on the grains and more exothermic recombinations), and can be incorporated into our effective sticking formalism if the desorption rate coefficient is roughly independent of species. Both our low effective sticking probability and desorption caused by internal processes operate throughout the disk.

The other group involves external particles or radiation, such as cosmic rays, UV photons, and X-rays. In this case the desorption rate per species is determined by the flux of energetic particles or radiation, and does *not* depend formally on the gas density. These mechanisms can maintain a steady state in which some portion of species, especially the most volatile ones CO and N_2, exists in the gas. A larger portion of molecules can stay in the gas phase in the surface or intermediate region of the disk, in which the radiation flux is larger and the gas density (and thus the adsorption rate per unit volume) is lower. Desorption rates by interstellar X-rays and cosmic rays have been estimated previously (Léger et al. 1985); the gas phase abundance is significant only in a region with $n_{\rm H} \lesssim 10^4\ cm^{-3}$. However, the desorption rate is dependent on the grain size, and may be higher if the grains have smaller size or fractal structure, rather than a spherical shape assumed in Léger et al. (1985) (Bergin 1998, personal communication). The fact that our model at 3–$10\ 10^5$ yr shows reasonable agreement with the observational data indicates that this type of non-thermal desorption must be efficient in regions of the disk with density $n_{\rm H} \lesssim 8\ 10^5\ cm^{-3}$, if it is the main desorption mechanism. It should also be noted that the molecular column densities are less dependent on time than in our model if the gas-phase molecules are maintained by this type of desorption mechanism.

4.3. Dust sedimentation and growth

Sedimentation onto the midplane and collisional growth of dust particles are critical phenomena in the formation of planetary systems, because planets, including Jovian planets, are made from solid cores of rock and ice. Grain growth and sedimentation can occur sequentially or together. Although much theory has been done on the mechanism and time scale for the growth of dust particles (Nakagawa et al. 1981; Weidenschilling & Cuzzi 1993; Weidenschilling 1997), we do not have observational data

to challenge the theories. It would be interesting to see if molecular abundances can be used as a probe of the growth and sedimentation of dust.

The most important effect of sedimentation and grain growth on the chemistry is through UV shielding. Since UV radiation is attenuated mainly by grains, the radiation will penetrate more deeply into the disk once the total cross section of grains become smaller due to sedimentation and growth. The enhanced radiation field will generally make photodissociation and photoionization within the disk more rapid. In order to determine the size of this effect on the column density of various kinds of molecules, and to determine which species can be good probes, we have performed a calculation with a smaller shielding factor. In particular, the hydrogen column density corresponding to $A_{\rm v} = 1$ mag has been set to be $1.8\ 10^{22}\,{\rm cm}^{-2}$, which is one order of magnitude higher than the value for normal interstellar grains (Duley & Williams 1984). In the calculation, we have used the minimum-mass disk model, and have neglected ionization by X-rays. Although the adsorption rate of molecules onto grains will be lowered if grains grow significantly, we have used the same adsorption rate as in the original models in order to isolate the effect of photoprocesses.

The last column of Table 2 shows molecular column densities with the reduced dust-shielding at $R = 700$ AU and $t = 3\ 10^5$ yr. The effect of the reduced shielding can be seen by comparing this column with Column 3. The column densities of molecules such as N_2, O_2, NO, CO_2, H_2O, HCN, HNC, and NH_3 are reduced significantly. The column density of CO is not much changed, because it is mainly shielded by H_2 and CO itself. Thus abundance ratios such as $\Sigma({\rm HNC})/\Sigma({\rm CO})$ and $\Sigma({\rm NH_3})/\Sigma({\rm CO})$ can be probes for sedimentation; observation of these and other molecular abundance ratios in many disk systems may enable us to estimate the time scale of grain growth. If we reduce the adsorption rate as dust particles grow, the absolute value of the molecular column densities will be higher than we estimate here, but the ratios $\Sigma({\rm HNC})/\Sigma({\rm CO})$ and $\Sigma({\rm NH_3})/\Sigma({\rm CO})$ will remain unchanged.

The effect of sedimentation bears some resemblance to the effect of lowering the disk mass, so that it would be difficult to determine both the disk mass and sedimentation degree at the same time from molecular observations only. For DM Tau, an independent measurement of the disk mass exists so that a less massive disk model is forced upon us. Since our model without sedimentation is in good agreement with observation in the DM Tau system, there is no evidence for sedimentation here. Observation of molecular ratios such as $\Sigma({\rm HNC})/\Sigma({\rm CO})$ and $\Sigma({\rm NH_3})/\Sigma({\rm CO})$ towards various objects with different ages should enable us to estimate the time scale for dust sedimentation statistically.

4.4. Effect of mixing

Although we have neglected hydrodynamic motions within the disk for simplicity, turbulence or accretion flow can cause mixing or migration of matter. Here we discuss the likely effect of mixing on the molecular column densities.

First, consider turbulent mixing in the Z-direction with a turbulence velocity $v_{\rm turb}$ and a mixing length or size of the largest eddies $l_{\rm turb}$. The mixing time of matter (yr) via random walk processes is given by

$$\tau_{\rm mix}^{(Z)} \approx \frac{H^2}{l_{\rm turb} v_{\rm turb}} \approx 2\times 10^5 \left(\frac{R}{600{\rm AU}}\right)^{3/2} \left(\frac{0.1H}{l_{\rm turb}}\right) \left(\frac{0.1C_{\rm s}}{v_{\rm turb}}\right), \quad (10)$$

where H is the scale height of the disk and $C_{\rm s}$ is the sound velocity (e.g. Aikawa et al. 1996). At $R \gtrsim 600$ AU, the mixing time is comparable to the age of the disk, which is $(3\text{–}10)\ 10^5$ yr for the disks in which we are interested, and is smaller than the disk age for inner regions. Thus the mixing will not drastically change our results for the outermost disk regions ($R \gtrsim 600$ AU), although the effect may be more serious in the inner regions. The effect of mixing in the Z-direction depends on the efficiency of non-thermal desorption in the regions removed from the midplane. If there is no effective desorption mechanism, the net result will be a decrease of the abundances of gas-phase molecules due to depletion onto grains in the midplane. When the adsorbed matter is transported back to the surface or intermediate regions, the gas-phase abundances remain low. If, however, there is an effective mechanism for non-thermal desorption away from the midplane, or if the temperature is high enough to desorb molecules, then the calculated molecular column densities will not change much from our current results because of the rapid time scale of the ensuing gas-phase chemistry compared with the mixing time.

There is also the possible effect of radial mixing or accretion flow towards the central star. The most important parameter which varies in the radial direction is temperature. Fig. 7 shows that the column densities of carbon-bearing molecules are almost constant at $R \gtrsim 200$ AU, and increase at $R \sim 200$ AU, because the temperature at this region is equal to the sublimation temperature of CO (the so-called "sublimation front"), which is the most abundant form of vaporizable carbon. Thus we can expect that the column densities of carbon-bearing molecules such as those shown in Fig. 7 do not change much as long as the accretion flow does not cross the sublimation front. If the matter migrating inwards crosses the sublimation front, however, the CO sublimates abruptly, and other carbon-bearing molecules begin to be formed from the sublimated CO. Since it takes some time, about $t \sim 10^4$ yr in the intermediate Z regions for example, for the gas-phase chemistry to reach steady state (Fig. 5), a rapid accretion flow across the sublimation front will transport the lower abundances of the outer regions into the inner regions so that the molecular column densities at $R \lesssim 200$ AU will be smaller than shown in Fig. 7. The width of the transient zone depends on the chemical time scale and accretion velocity (Aikawa et al. 1999). Assuming a chemical time scale $\sim 10^4$ yr and accretion velocity 10^{-3} AU yr^{-1}, which corresponds to $\alpha \sim 0.1$ in the α-prescription of the viscosity given by Shakura & Sunyaev (1973), the width is rather small ~ 10 AU, for example. If matter migrates rapidly outward across the sublimation front, on the other hand, a similar analysis suggests that the molecular

column densities at $R \gtrsim 200$ AU would be higher than shown in Fig. 7 although the calculation of the transient zone would depend on the adsorption rate. In other words, the molecular column densities near the sublimation front of CO would be more averaged in the R-direction if there is some mechanism for radial mixing. Observational studies of molecules at this radius can help to determine the importance of such mixing, although small transient zones could not be discerned with the current generation of interferometers.

5. Summary

We have investigated the two-dimensional (R, Z) distribution of molecules in circumstellar disks around young stellar objects. On the midplane, in cool outer regions of a disk, most of the molecules are adsorbed onto grains within a short time and depleted from the gas phase owing to the high density. As the height Z increases, the density decreases and the time scale for adsorption of molecules onto the dust particles increases. At the outermost layers, known as the surface regions, molecules are dissociated by UV radiation. Hence, with the standard values for the lifetime of young stellar objects, the molecular abundances have their peak values at some intermediate region. The height at which the abundances reach their peak values varies with species. Radicals, such as CN and C_2H, have their peaks at larger heights Z compared with more stable species such as HCN and NH_3. The chemistry in regions removed from the midplane is also affected by X-ray ionization if the central star is a strong X-ray emitter. The abundances of most molecular species are slightly higher in the case of X-ray ionization, since the increased ionization leads to more ions and more rapid ion-based syntheses.

By integrating molecular abundances in the Z-direction, we obtain column densities of molecules as functions of disk radius R. Our model is consistent with observational data for most of the molecules detected by Dutrey et al. (1997) in DM Tau. A salient feature of our calculated radial distributions for column densities is that for many carbon-bearing species there is a strong increase in column density at or near the so-called sublimation front of CO, which occurs at $R \approx 200$ AU. This prediction is most valid in the absence of rapid radial mixing across the sublimation front. Vertical mixing caused by turbulence has an uncertain effect on our calculated column densities which depends on the efficiency of non-thermal desorption of dust mantles.

Species such as HNC, NH_3, HCO^+, and H_3O^+ are particularly sensitive to the total column density of the disk; in a less massive disk, where the shielding of UV radiation is less effective, these molecules are destroyed more efficiently. Sedimentation and growth of dust particles also affect the chemistry by changing the UV radiation field in the disk. Species such as N_2, O_2, NO, CO_2, H_2O, HCN, HNC, and NH_3 are sensitive to these effects. Reducing the disk mass and including sedimentation and grain growth often have similar effects on the molecular column densities, although some molecules show different behavior owing to the lower density in the less massive disk. Carbon monoxide is not much affected by either a change in disk mass or sedimentation, so that abundance ratios such as Σ(HNC)/Σ(CO) and $\Sigma(NH_3)/\Sigma$(CO) can be a useful probe to investigate disk mass or sedimentation. A statistical study of these ratios towards various objects with different ages will enable us to estimate the time scale of dust sedimentation.

Acknowledgements. The authors are grateful to Profs. S. M. Miyama, T. Umebayashi, and T. Nakano for helpful discussions. Y. A. is grateful for financial support of the Japan Society for Promotion of Science. The Astrochemistry Program at The Ohio State University is supported by The National Science Foundation. Numerical calculations were carried out on the Cray T90 at the Ohio Supercomputer Center.

References

Adams F.C., Lin D.N.C., 1993, In: Levy E.H., Lunine J.I. (eds.) Protostars and Planets III. Univ. of Arizona Press, Tucson, p. 721
Aikawa Y., Herbst E., 1999, ApJ in press
Aikawa Y., Miyama S.M., Nakano T., Umebayashi T., 1996, ApJ 467, 684
Aikawa Y., Umebayashi T., Nakano T., Miyama S.M., 1997, ApJ 486, L51
Aikawa Y., Umebayashi T., Nakano T., Miyama S.M., 1998, In: Chemistry and Physics of Molecules and Grains in Space. The Royal Society of Chemistry, London, p. 281
Aikawa Y., Umebayashi T., Nakano T., Miyama S.M., 1999, ApJ 519, 705
Anders E., Grevesse N., 1989, Geochimica et Cosmochimica Acta 53, 197
Beckwith S.V.W., Sargent A.I., Chini R.S., Güsten R., 1990, AJ 99, 924
Cameron A.G.W., 1973, Space Sci. Rev. 15, 121
Caselli P., Hasegawa T.I., Herbst E., 1998, ApJ 495, 309
d'Hendecourt L.B., Allamandola L.J., Baas F., Greenberg J.M., 1982, A&A 109, L12
Duley W.W., Williams D.A., 1984, Interstellar Chemistry. Academic Press, New York
Dutrey A., Guilloteau S., Simon M., 1994, A&A 286, 149
Dutrey A., Guilloteau S., Guélin M., 1997, A&A 317, L55
Finocchi F., Gail H-P., 1997, A&A 327, 825
Glassgold A.E., Najita J., Igea J., 1997, ApJ 480, 344
Gredel R., Lepp S., Dalgarno A., Herbst E., 1989, ApJ 347, 289
Guilloteau S., Dutrey A., 1994, A&A 291, L23
Guilloteau S., Dutrey A., 1998, A&A 339, 467
Handa T., Miyama S. M., Yamashita T., et al., 1995, ApJ 449, 894
Hasegawa T.I., Herbst E., 1993, MNRAS 261, 83
Hayashi C., 1981, Prog. Theor. Phys. Suppl. 70, 35
Herbig G.H., Goodrich R.W., 1986, ApJ 309, 294
Imhoff C.L., Appenzeller I., 1987, In: Kondo Y. (ed.) Scientific Accomplishments of the I. U. E., Reidel, Dordrecht, p. 295
Kawabe R., Ishiguro M., Omodaka T., Kitamura Y., Miyama S.M., 1993, ApJ 404, L63
Koerner D.W. Sargent A.I., 1995, AJ 109, 2138
Koerner D.W., Sargent A.I., Beckwith S.V.W., 1993, Icarus 106, 2
Koyama K., Maeda Y., Ozaki M., et al., 1994, PASJ 46, 125
Lee H.-H., Herbst E., Pineau des Forêts, G., Roueff E., Le Bourlot J., 1996, A&A 311, 690
Lee H.-H., Roueff E., Pineau des Forêts G., et al., 1998, A&A 334, 1047
Léger A., Jura M., Omont A., 1985, A&A 144, 147
Maloney P., Hollenbach D.J., Tielens A.G.G.M., 1996, ApJ 466, 561

Montmerle T., Feigelson E.D., Bouvier J., André P., 1993, In: Levy E.H., Lunine J.I. (eds.) Protostars and Planets III. Univ. of Arizona Press, Tucson, p. 689
Nakagawa Y., Nakazawa K., Hayashi C., 1981, Icarus 45, 517
Osamura Y., Fukuzawa K., Terzieva R., Herbst E., 1999, ApJ 519, 697
Ruffle D.P., Hartquist T.W., Taylor S.D., Williams D.A., 1997, MNRAS 291, 235
Ruffle D.P., Hartquist T.W., Williams D.A., 1999, MNRAS 306, 691
Saito M., Kawabe R., Ishiguru M., et al., 1995, ApJ 453, 384
Sandford S.A., Allamandola L.J., 1993, ApJ 417, 815
Shakura N.I., Sunyaev R.A., 1973, A&A 24, 37
Shalabiea O.M., Caselli P., Herbst E., 1998, ApJ 502, 652
Skrutskie M.F., Snell R.L., Strom K.M., et al., 1993, ApJ 409, 422
Suzuki H., 1983, ApJ 272, 579
Terzieva R., Herbst E., 1998, ApJ 501, 207
Umebayashi T., Nakano T., 1981, PASJ 33, 617
van Dishoeck E., Black J., 1988, ApJ 334, 771
Weidenschilling S.J., 1997, Icarus 127, 203
Weidenschilling S.J. Cuzzi J.N., 1993, In: Levy E.H., Lunine J.I. (eds.) Protostars and Planets III. Univ. of Arizona Press, Tucson, p. 1031
Willacy K., Millar T.J., 1998, MNRAS 298, 562
Willacy K., Klahr H.H., Millar T.J., Henning T.H., 1998, A&A 338, 995
Williams D.A., 1993, In: Millar T.J., Williams D.A. (eds.) Dust and Chemistry in Astronomy. Institute of Physics Publishing, London, p. 143
Yamamoto T., Nakagawa N., Fukui Y., 1983, A&A 122, 171